Journal of Atmospheric and Solar-Terrestrial Physics 121 (2014) 32–41

Contents lists available at ScienceDirect

Journal of Atmospheric and Solar-Terrestrial Physics

journal homepage: www.elsevier.com/locate/jastp

Global simulation of extremely fast coronal mass ejection on 23 July 2012

Kan Liou [a,*], Chin-Chun Wu [b], Murray Dryer [c], Shi-Tsan Wu [d], Nathan Rich [b], Simon Plunkett [b], Lynn Simpson [b], Craig D. Fry [e], Kevin Schenk [f]

[a] Johns Hopkins University Applied Physics Laboratory, Laurel, MD 20723, USA
[b] Naval Research Laboratory, Washington, DC 20375, USA
[c] NOAA Space Weather Prediction Center (Ret.), Boulder, CO 80305, USA
[d] CSPAR, University of Alabama, Huntsville, AL 35899, USA
[e] Exploration Physics International, Inc., Huntsville, AL 35806, USA
[f] NASA/GSFC, Greenbelt, MD, USA

ARTICLE INFO

Article history:
Received 21 November 2013
Received in revised form
12 September 2014
Accepted 23 September 2014
Available online 30 September 2014

Keywords:
Coronal mass ejection
MHD simulation
CME-driven shock

ABSTRACT

The July 23, 2012 CME was an extremely fast backside event, reaching ~1 AU (STEREO-A) within 20 h as compared to ~3–6 days for typical CME events. Here, we present results from a simulation study of the CME and its driven shock using a combined kinematic and magnetohydrodynamic (MHD) simulation model, H3DMHD. In general, the model results match well with in situ measurements in the arrival time of the CME-driven shock and the total magnetic field strength, assuming an initial CME speed of 3100 km/s. Based on extrapolation of an empirical model, the fast CME and its large magnetic field ($|\boldsymbol{B}|$~120 nT) are capable of producing an extremely large geomagnetic storm (Dst~−545 nT), comparable to the well-known Halloween storm in 2003, if the CME had made a direct impact to the Earth. We investigated the effect of the adiabatic index (γ). It is found that the shock tends to arrive slightly later for a smaller γ value, and $\gamma=5/3$ provides the best agreement for the shock arrival time. We also demonstrate that the strength (the Mach number) of the CME-driven fast-mode shock is not the largest at the "nose" of the CME. This is mainly due to the manifestation of fast-mode wave speed upstream of the shock.

1. Introduction

Coronal mass ejections (CMEs) are eruptions of magnetized plasma from the solar atmosphere into the interplanetary space, where they are often referred to interplanetary CMEs (ICMEs). Since their first observations in the 1970s with white light imagers (Tousey, 1973; MacQueen et al., 1980), CMEs/ICMEs have drawn much attention for their adverse space weather effects. For example, solar energetic particle (SEP) events of a gradual type are believed to be accelerated by fast-mode shocks driven by CMEs (see review by Reams (1999)). Geomagnetic storms often occur after the arrival of an ICME at the Earth (Gosling et al., 1991). Statistical studies have indicated that the majority of front-site CMEs can hit the Earth (Yermolaev and Yermolaev, 2006) and induce geomagnetic storms (see review by Akasofu (2011)).

The average speed of CMEs derived from white light coronagraph data ranges from 300 km/s during solar minimum to 500 km/s during solar maximum (Yashiro et al., 2004; Gopalswamy et al., 2005), which translates to ~3–6 days for a typical CME to reach 1 AU. However, fast CMEs with a propagation speed greater than 900 km/s are not uncommon, averaging ~13% (Yashiro et al., 2004). Those fast and mostly Halo-CMEs can reach the Earth in ~2 days. Historically, there are no more than 13 documented solar events that propagated to Earth in less than 1 day (Cliver and Svalgaard, 2004), and there are only a few historical events with the shock transit times less than 20 h. Notably speaking, the shock from the August 4, 1972 event (e.g., Zastenker et al., 1978), with a transit time of ~14.6 h, is considered to be the fastest ICME (interplanetary coronal mass ejection) event on record. The solar flare that was associated with the "superstorm" of September 1, 1859 also took less time (17.6 h) (Carrington, 1859). The "Halloween-events" in 2003 belong also to the few extremely fast ICME events (Skoug et al., 2004).

* Corresponding author. Fax: +1 4109641641.
E-mail address: kan.liou@jhuapl.edu (K. Liou).

http://dx.doi.org/10.1016/j.jastp.2014.09.013
1364-6826/

In addition to a frontal (fast-mode) shock and an ejecta, a typical CME also consists of a magnetic cloud (MC) (Burlaga et al., 1981). The large magnetic fields associated with MCs and cloud sheath are responsible for large geomagnetic storms (e.g., Wu and Lepping, 2002; Zhang et al., 2004). During solar cycle 23, the average intensity of geomagnetic storms associated with MCs and ICMEs is ~13 and 10 nT, respectively (Wu and Lepping, 2011). The magnetic field associated with the Halloween CME events was ~60 nT (Skoug et al., 2004). Such an unusually large magnetic field was responsible for the severe Halloween storm events.

Large magnetic storms are often associated with earthward moving halo-CME events (e.g., Badruddin, 2013), as there is a greater chance for halo-CMEs than non-halo-CMEs to make a direct impact to the Earth. On the other hand, a CME that occurs on the back side of the Sun from the Earth (backside CMEs) is not likely to reach the Earth no matter how large the event is. The CME event that occurred on July 23, 2012 represents one such an event. The CME was considered "extremely fast" because it reached 1 AU in ~20 h as recorded by STEREO-A and resulted in no geomagnetic effect on the Earth (Dryer et al., 2012; Russell et al., 2013; Baker et al., 2013). From the perspective of space weather, farside or even backside CME events such as the July 23 event can pose threats to spacecraft nearby or along CME trajectories. For example, the Messenger spacecraft is currently orbiting Mercury (~0.37–0.47 AU from the Sun), and the planned European Space Agency's Solar Orbiter will have orbits ~0.25 AU from the Sun and NASA's Solar Probe Plus will fly as close as $9.8R_S$ from the Sun. The lead time will be too short for these spacecraft to react.

In this paper, we will present results from our study of this solar flare/shock/CME event using global simulation. While we will focus on the characteristics of the July 23, 2012 event, the extremely fast CME event allows us to test the capability of the simulation code. The rest of the paper is organized as follows. We will discuss the observations in Section 2, simulation model in Section 3, followed by simulation and validation of results in Section 4. Discussion of the results and conclusions are given in Sections 5 and 6, respectively.

2. Observations

The present "extremely rare" event was, to our knowledge, first described by Dryer et al. (2012) because of its exceptionally fast speed and MC field characteristics. Fig. 1 shows the locations of the STEREO Ahead (0.963957, 345.633°, 1.750°)/Behind (1.021173, 109.567°, −6.979°) and the Earth (1.015935, 224.386°, 5.08°) relative to the CME initiation site at 00:00 UTC in the heliospheric Earth ecliptic (HEE) coordinate (AU, longitude, latitude) system. The longitudinal separation of the STEREO-A and the STEREO-B spacecraft with the Earth was 120.912° and 115.200°, respectively. The separation angle between STEREO-A and STEREO-B was 123.887°. The July 23, 2012 CME event was initiated from the active region AR-1520 on the Sun's back side. Fig. 2((a) and (b)) shows two consecutive solar disk images in 19.5 nm from the Extreme Ultraviolet Imager (EUVI) on STEREO-A—one before (a) and one after (b) the onset of the CME. The onset of the CME can be identified as a sudden brightening within the active region AR-1520 at S16W133 (pointed by an arrow in Fig. 2(b)). Because it is a backside event, its associated flare was not visible to the frontside observers such as the GOES satellites. On the other hand, the small (~12°) longitudinal separation between the CME onset location and STEREO-A makes it a standard halo-CME when observed at STEREO-A. From the STEREO-B, it appears to be a partial halo-CME. Fig. 2((c) and (d)) shows two coronagraph images from STEREO-A/COR2 and STEREO-B/COR2, respectively,

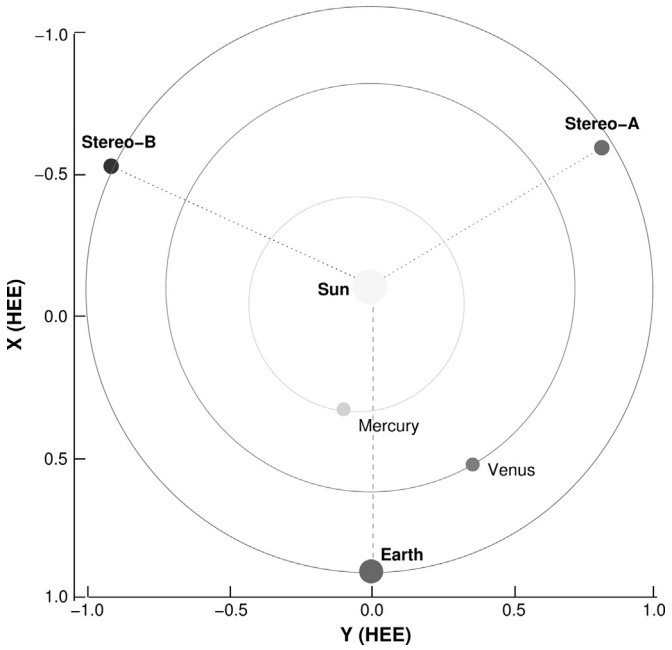

Fig. 1. The positions of the STEREO-A and STEREO-B spacecraft relative to the Sun and Earth in heliocentric Earth ecliptic (HEE) coordinate system at July 23, 2012 03:00 UT. The dotted lines show the angular displacement from the Sun. Units are in AU.
(Information obtained from NASA's Stereo Science Center)

taken several minutes after the CME onset (~02:50 UT). The brighter CME in the STEREO-A/COR2 image (Fig. 2(c)) indicates that the CME source is in the southern hemisphere (~S16°).

3. Simulation model

This study employs a "hybrid" simulation model (H3DMHD) of Wu et al. (2007) to simulate the CME event. The model combines an updated version of the kinematic code of Hakamada–Akasofu–Fry (HAFv.2) (see Fry et al., 2001, and references therein) and a three-dimensional (3-D), time-dependent numerical MHD model (Han et al., 1988). The HAFv.2 code, an improved version of the HAF code originally developed by Hakamada and Akasofu (1982), is used to handle the simulation for subsonic/sub-Alfvénic flows in the inner and outer coronal region sunward of $18R_S$, while the MHD code is used to simulate supersonic and super-Alfvénic MHD flows, i.e., outside of the critical surface of Parker's solar wind model. The two simulation codes are joined at $18R_S$, where the output of HAFv.2 is fed into the MHD code's time-dependent inner boundary values.

Simulation of solar wind and CMEs in supersonic/super-Alfvénic solar wind flows is carried out by a time-dependent, 3-D, MHD numerical code originally developed by Han (1977). The code solves a set of ideal MHD equations that exclude the Coriolis force, Joule heating, thermal conduction, and viscous terms. The MHD equation sets, from Eqs. (1)–(4) listed below, are conservation of mass, conservation of momentum, conservation of energy, and magnetic induction:

$$\frac{D\rho}{Dt} + \rho\nabla\cdot\boldsymbol{V} = 0 \tag{1}$$

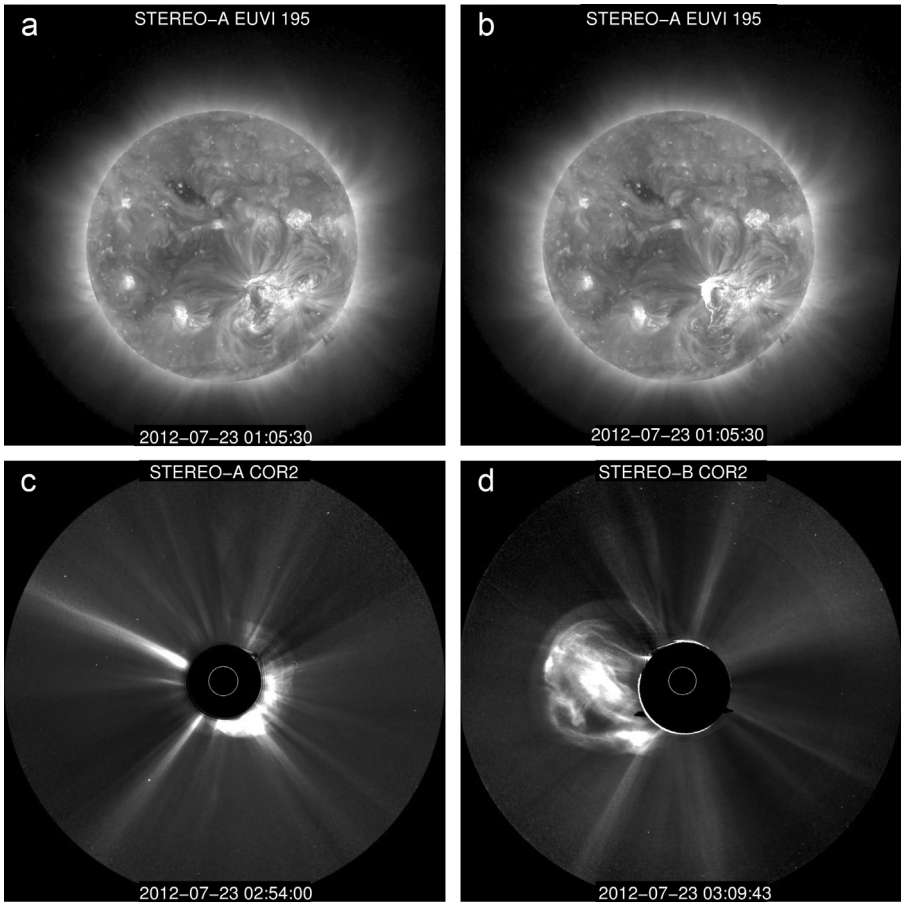

Fig. 2. ((a) and (b)) Solar EUV disk images from STEREO-A and; (c) and (d) are coronagraph images from STEREO COR2A and COR2B, respectively for the July 23, 2012 coronal mass ejection (CME) event. The arrow in (b) points at the CME onset.

$$\rho\frac{D\boldsymbol{V}}{Dt} = -\nabla p + \frac{1}{\mu_0}(\nabla\times\boldsymbol{B})\times\boldsymbol{B} - \rho\frac{GM(r)}{r^2}\hat{\boldsymbol{r}} \tag{2}$$

$$\frac{\partial}{\partial t}\left(\rho e + \frac{1}{2}\rho V^2 + \frac{B^2}{2\mu_0}\right) + \nabla\cdot\left[V\left(\rho e + \frac{1}{2}\rho V^2 + p\right) + \frac{\boldsymbol{B}\times(\boldsymbol{V}\times\boldsymbol{B})}{\mu_0}\right] = -\boldsymbol{B}\cdot\frac{\rho \mathrm{GM}(r)}{r^2}\hat{\boldsymbol{r}} \tag{3}$$

$$\frac{\partial\boldsymbol{B}}{\partial t} = \nabla\times(\boldsymbol{V}\times\boldsymbol{B}) \tag{4}$$

where D/Dt denotes the time total derivative, ρ, $\boldsymbol{V}$, and p are the mass density, velocity, and thermal pressure of the MHD fluid, respectively, $\boldsymbol{B}$ is the magnetic field strength, e is the internal energy per unit mass ($=p/[\rho(\gamma-1)]$), $GM(r)/r^2$ is the solar gravitational force as a function of the radial distance, r, from the center of the Sun, and γ is the specific heat ratio (C_P/C_V). In this study, an adiabatic MHD fluid with the specific heat ratio of $\gamma=5/3$ is assumed. We also test different values of γ to understand its effect.

The H3DMHD model uses a Sun-centered spherical coordinate system (r, θ, φ). The computational domain is set to $2.5\le r\le 285R_S$, $-87.5^\circ\le\theta\le 87.5^\circ$, and $0^\circ\le\varphi\le 360^\circ$, with uniform grids: $\Delta r=3R_S$, $\Delta\theta=5^\circ$, and $\Delta\varphi=5^\circ$. The outer boundary condition is of a non-reflective type, whereas the inner boundary is dynamically driven by a prescribed photospheric field (r-component only) and solar wind velocity (Arge and Pizzo, 2000). The two angular grid sizes are chosen to match the spatial resolution of the photospheric field. The radial grid size is chosen with efficiency of the code in mind while small enough to resolve the CME structure. The model uses the two-step Lax–Wendroff finite difference scheme to provide second order accuracy in both space and time (Lax and Wendroff, 1960). A detailed description of the numerical scheme can be found in the work of Han et al. (1988) and Detman et al. (1991).

The nonuniform background solar wind plasma and IMF are essential for the coupling of the corona to the solar wind. We first use this model to simulate pre-event steady state solar wind based on solar magnetic maps. Then we apply a Gaussian velocity pulse at the inner boundary to simulate the CME. The velocity pulse is parametrized by the width (duration) and the height (amplitude). The duration of the flare measured by the GOES X-ray instruments is used as a proxy for the duration. However, for this backside event, direct flare observations from Earth are not available. We use a time duration of 3.5 h, which is typical for large X-ray flares, for this event. The height of the velocity pulse, i.e., the initial speed of the CME, is obtained from the coronagraph observations. The relation of CME and shock speed can be provided by analogy with the laboratory shock tube's "piston" and its shock (Dryer, 1981).

In this study we use a coronagraph analysis software tool developed by the Naval Research Laboratory to estimate the speed of the CME. Here, as an example, we used a sequence of 6 coronagraph images from SOHO/LASCO C2/C3 (Brueckner et al., 1995) to measure the CME propagation front, marked with an "s" in Fig. 3(a). By multiplying the location of the selected pixels to the cosine of the position angle, the radial distance of the propagation front is calculated (see Sheeley et al., 2008, for details). These measurements were performed ten times in order to determine the stand deviation and the mean values of the height profile. After applying a linear least-squares fit, we obtain an initial CME/

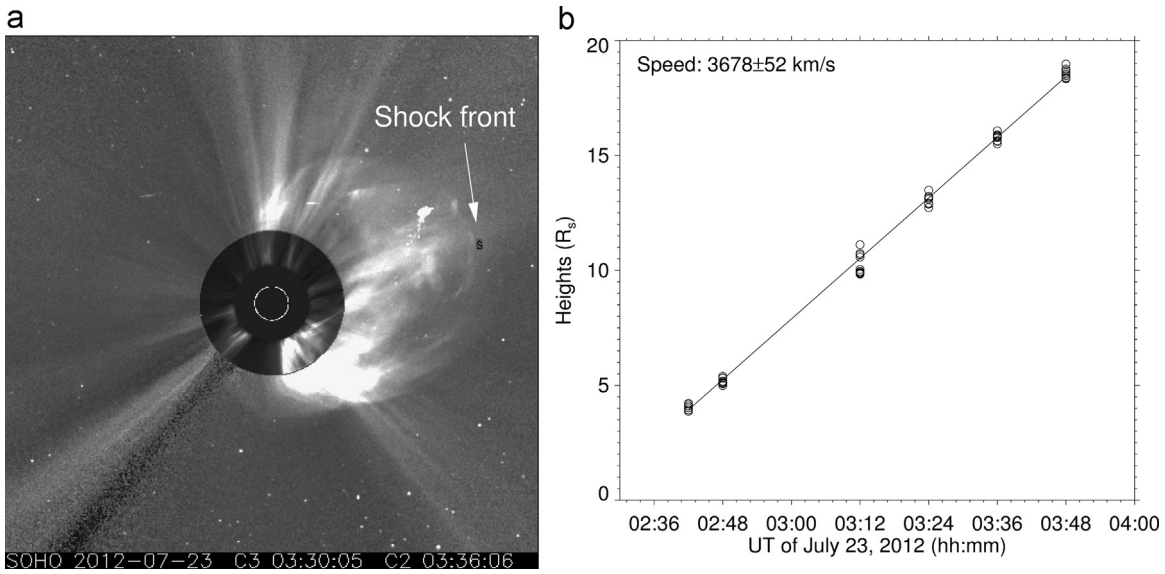

Fig. 3. (a) An example of SOHO/LASCO composite image from C2 and C3. (b) Linear regression analysis of time series of CME/shock locations. The CME/shock location is estimated by tracking the CME/shock front on each of the SOHO/LASCO C2/C3 images marked as an "s" on (a).

shock speed of 3678 ± 52 km/s (Fig. 3(b)). The small uncertainty (1-standard deviation) relative to the average value suggests that consistent results can be obtained from this analyzing procedure. This speed is close to the initial shock speed estimated with the STEREO-A coronagraph images using the same method (Dryer et al., 2012). Note that different speeds may result if different CME bright features are selected and tracked, and the propagation speed estimated from this method highly depends on δ because it is a free parameter and is assumed to be (δ) to range from 4.6° to 6.8° ($5.7 \pm 0.8°$). Therefore, this procedure can only provide ballpark figures for the initial CME speed. In this simulation we use 2900 km/s as the CME initial speed and adjust (i.e., "tune") the value by 100 km/s increments if necessary until the difference between the simulated and true shock arrival times at STEREO-A is

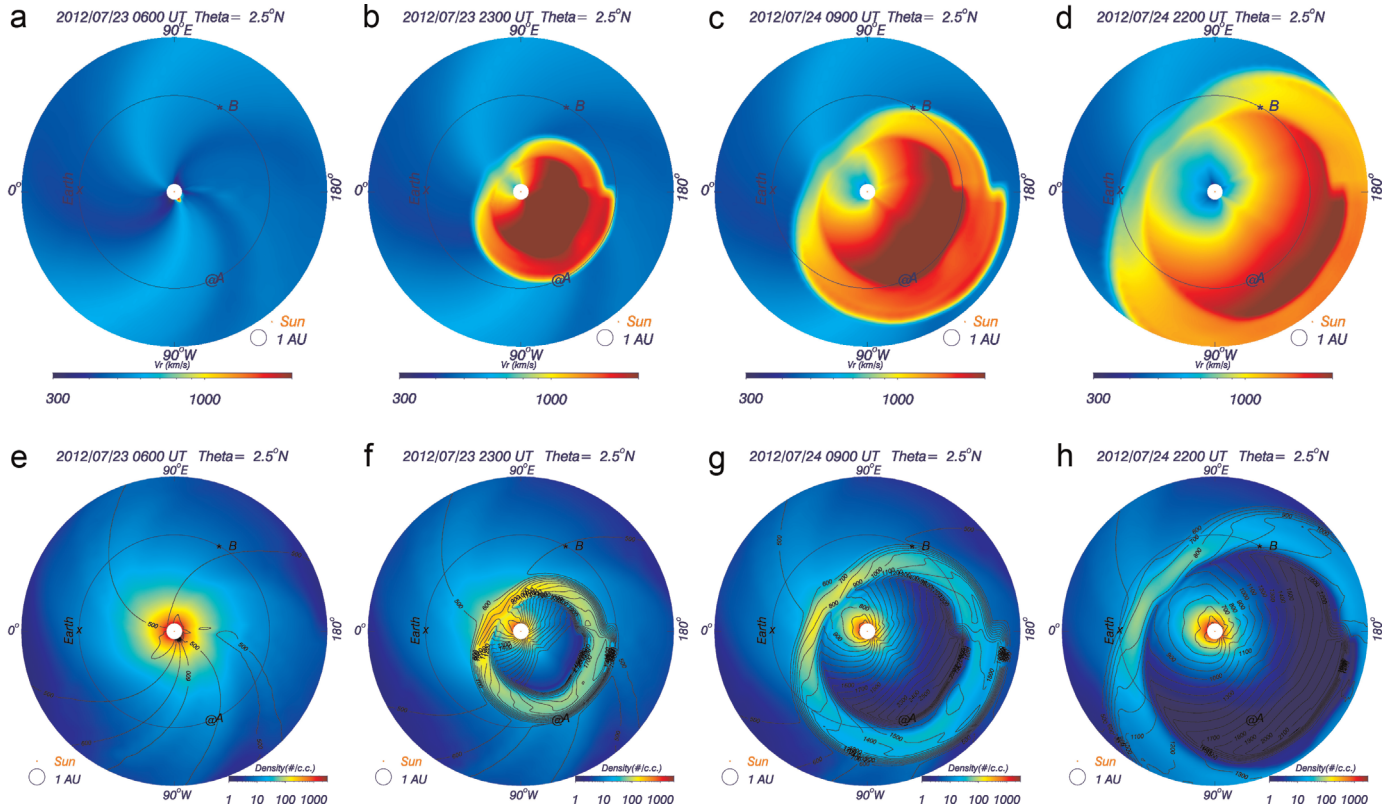

Fig. 4. ((a)–(d)) Simulated solar wind speed and CME at four times en route to 1.3 AU; (e–h) solar wind plasma density (color) and speed (black contours). (For interpretation of the references to color in this figure legend, the reader is referred to the web version of this article.)

small. It is found that 3100 km/s for the initial speed of the CME gives the best agreement. We will show detailed results in the following section.

4. Simulation results

4.1. General result

To demonstrate the global structure of the simulated CME and its evolution, we plot the radial speed and the density of the CME at the Sun's equatorial plane ($\theta=0°$) in Fig. 4. The heliocentric Earth ecliptic (HEE, X=Sun–-Earth line, Z=ecliptic north pole) coordinate system is used. Note that the Earth and STEREO-A/B were not located exactly on but up to ~7° from the equatorial plane. Because the actual location of STEREO-B is one grid (5°) below and the Earth is one grid above the equatorial plane, we expect the difference should be small. Fig. 4(a) shows the radial speed of the solar wind 3 h after the lift-off of the CME at 06:00 UT on July 23. The simulated background solar wind reveals two fast streamers (~700 km/s) in a spiral configuration, with the Earth (longitude $\phi=0°$) in the low solar wind speed (~400 km/s) and the STEREO-A and STEREO-B in the transition region between the fast and slow solar winds. At this time, the CME was ~25 solar radii from the surface of the Sun and can be seen as a small red dot near the longitude of STEREO-A. Notice that the CME initiation site coincides with the source region of one of the fast streamers, which may have contributed to the overall CME propagation speed. Fig. 4(b) shows the time when the CME-driven shock arrived at the STEREO-A spacecraft at 23:00 UT on July 23. At this time the CME and its driven shock, refracting around the Sun, has expanded more than 180° in longitude—sometimes called a "hemisphere-buster". About 10 h later, the CME reached the STEREO-B spacecraft at 10:00 UT on July 24 (Fig. 4(c)), and another 12 h (22:00 UT on July 25) later the weakened eastern flank of the CME-driven shock arrived at the Earth (see Fig. 4(d)).

Fig. 4(e)–(h) shows four snapshots of solar wind density in a color-coded format at times similar to those for the solar wind speed shown in Fig. 4(a)–(d). The contour lines in black represent the velocity contours.

4.2. Validation with STEREO-A data

Comparing simulation results with in situ measurements constitutes a means to validate the simulation. Here, we compare simulated results with total magnetic strength data acquired from IMPACT/MAG (Acuna et al., 2008) and solar wind plasma density, temperature, radial speed from PLASTIC (Galvin et al., 2008), all on board STEREO-A. Note that because the photospheric field is assumed to be in the radial direction at $r=2.5R_S$, our model thus cannot simulate the realistic vector fields. This is also true for all data-driven global MHD simulations (e.g., Manchester et al. 2004; Odstrcil et al. 2005; Wu et al. 2007; Lugaz and Roussev 2011; Shen et al., 2011). Therefore, we can only compare the total magnetic field strength, which is a variable that can be simulated adequately. Fig. 5(a) shows the comparison of the field strength. As one can see, the arrival time of the sudden field increase (shock front) matches well (due to the empirical approach described in Section 1) with the simulated field. The simulated total field intensity peak is ~130 nT, which is reasonably in good agreement with the observed peak field intensity that reached 109 nT at a 1-min time scale (Russell et al., 2013). Note that although the output of our simulation is once per hour, the actual time step varies and can be as small as a few minutes.

Unfortunately, data from the PLASTIC plasma instrument on STEREO-A was compromised on July 24, as noted in the caption of

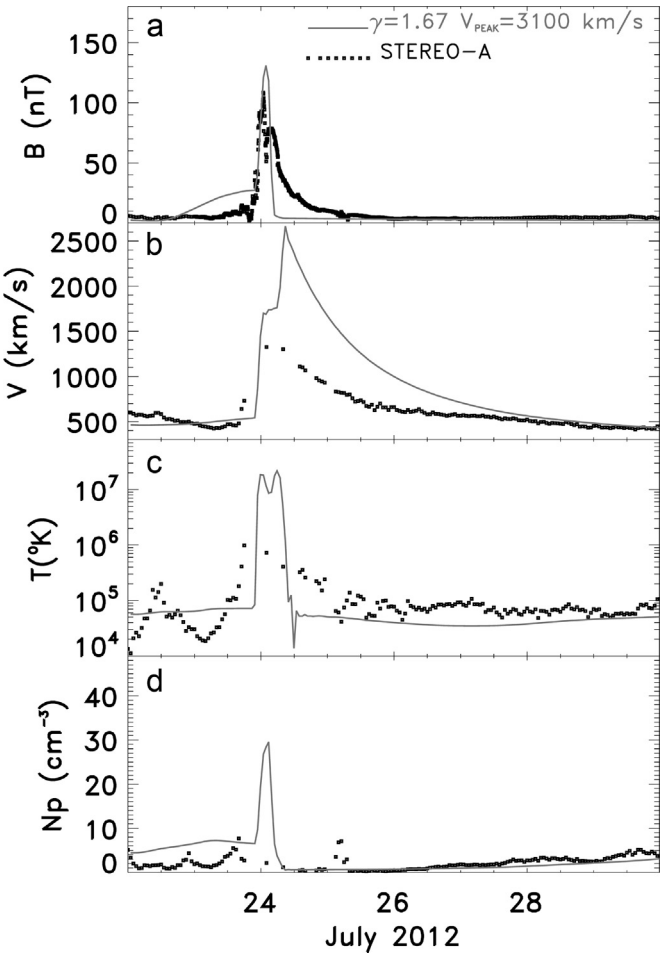

Fig. 5. Comparison of simulated (gray lines) and STEREO-A observational (black dots) data for (a) total magnetic field strength, (b) solar wind bulk flow speed, (c) temperature, and (d) the proton number density. Plasma data gaps exist on and around day 206 (July 24) due to instrument saturation. The simulation suggests that the second peak in the magnetic intensity is associated with a reverse shock.

Fig. 5, due to contamination by solar energetic particles. Therefore, we will only use the uncompromised part of the data as provided by the STEREO Science Center for comparison. Fig. 5(b) shows the hourly proton flow speed. In general, there is a good agreement in the upstream solar wind speed (~500 km/s) and the onset time of the sharp increase in the flow speed. However, there are differences in the flow structure. Prior to the arrival of the shock, there is a small increase in the solar wind flow speed from ~500 km/s to more than ~800 km/s at ~17 UT on July 23. This small pre-event perhaps also caused a small increase (peak $|\boldsymbol{B}|$~15 nT) in the total magnetic field. This small increase is not shown in our simulation result because we did not insert a perturbation corresponding to the pre-event conditions into our simulation. On the other hand, Russell et al. (2013) interpreted the small initial field increase as the arrival of the CME event and argued that the CME was not preceded by a fas-mode shock due to the very high pressure of the energetic particles. The simulated hourly flow speed at the shock downstream is ~1600 km/s and is slightly larger than the flow speed (~1300 km) at the corresponding time. Furthermore, our simulation shows an even larger flow speed at a much later time (~09 UT on July 24) than that observed. The simulated flow peak is associated with a reverse shock, but this cannot be confirmed by the compromised plasma density, velocity, and temperature. The second peak in $|\boldsymbol{B}|$ (see Fig. 5(a)) may be an evidence for the reversed shock, although it was measured ~7 h later (at ~0200 UT on July 24). On the other hand, Liu et al. (2014) suggested that the

July 23 CME event was associated with two "nearly simultaneous" eruptions and they may have contributed to the two-peak feature in the total magnetic field observed by STEREO-A. Fig. 5(c) and (d) shows the comparison of the solar wind proton temperature and density. There are large discrepancies in the solar wind plasma density and temperature.

Downstream of the shock, the simulated solar wind speed is about a factor of 2 larger than the observed speed but is gradually approaching and matching the background solar wind on July 27. The simulated solar wind density and temperature are in agreement with the measurements at this time. Note that the MHD model employed here is just an approximation of the solar wind and CME fluids and one should not expect a perfect fit between our simulation result and the observations. In addition, uncertainties in the input parameters can also contribute to the discrepancy. It is useful to understand the effect of each parameter in the simulation result to improve our better understanding of the MHD simulation.

4.3. Effects of the initial CME speed and the ratio of specific heats (γ)

As already mentioned, we perform our simulation for a number of initial CME speeds starting from 2900 km/s, with 100 km/s increments. It is found that an initial CME speed of 3100 km/s results in a good match in the shock arrival time with the in situ measurement at STEREO-A. While the initial CME speed plays an important role in the shock arrival time, the ambient solar wind is also an important controlling factor. Both gas dynamic and MHD models suggest that the shock-standoff distance (in front of the Earth's magnetospheric subsolar point) is a function of the sonic Mach number and the ratio of specific heats. This is further complicated by the fact that CMEs are not solid objects. Here, we will explore the effect of the ratio of specific heats on the shock arrival time.

For each initial CME speed (V_0), we apply three different values of the specific heat ratio (1.25, 1.45 and 1.67) to our simulation. The result is shown in Fig. 6. In terms of the shock arrival time, it is shown that the (γ, V_0) pair, (1.67, 3100 km/s), respectively, performs the best; other pairs lead to a delay of ~1–5 h. In general, a larger value of the initial CME speed results in a faster shock. Fig. 6 also shows that a larger value of γ leads to an earlier arrival of the shock. With regard to the shock amplitude (B and V), all parameters result in a larger magnetic field strength. The (γ=1.67, V_0=2900 km/s) pair seems to provide the best prediction of the shock magnetic field strength. Fig. 6 also shows that a faster initial CME speed leads to a larger magnetic field strength and solar wind speed, whereas a slower initial CME speed leads to a smaller value of the magnetic strength and solar wind speed.

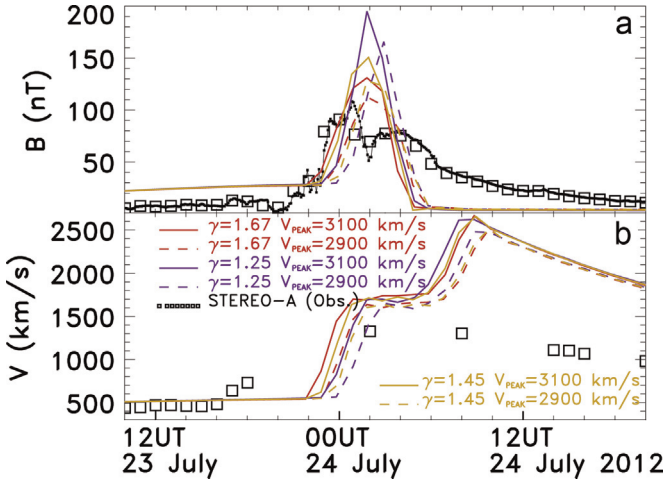

Fig. 6. Comparison of simulated (colors) and STEREO-A observational (black) results for a period from 12 UT on July 23 to 19 UT on July 24, 2012. The top panel shows the total magnetic field strength, whereas the bottom panel shows the solar wind bulk flow speed. Black squares are hourly averages of the STEREO data, whereas the black trace in the magnetic strength panel shows the 5-min averages of the data. Three specific heat ratios: γ=1.67 (red), 1.45 (gold), and 1.25 (blue), are used in combination with two initial CME speed: 3100 km/s (solid lines) and 2900 km/s (dashed lines). (For interpretation of the references to color in this figure legend, the reader is referred to the web version of this article.).

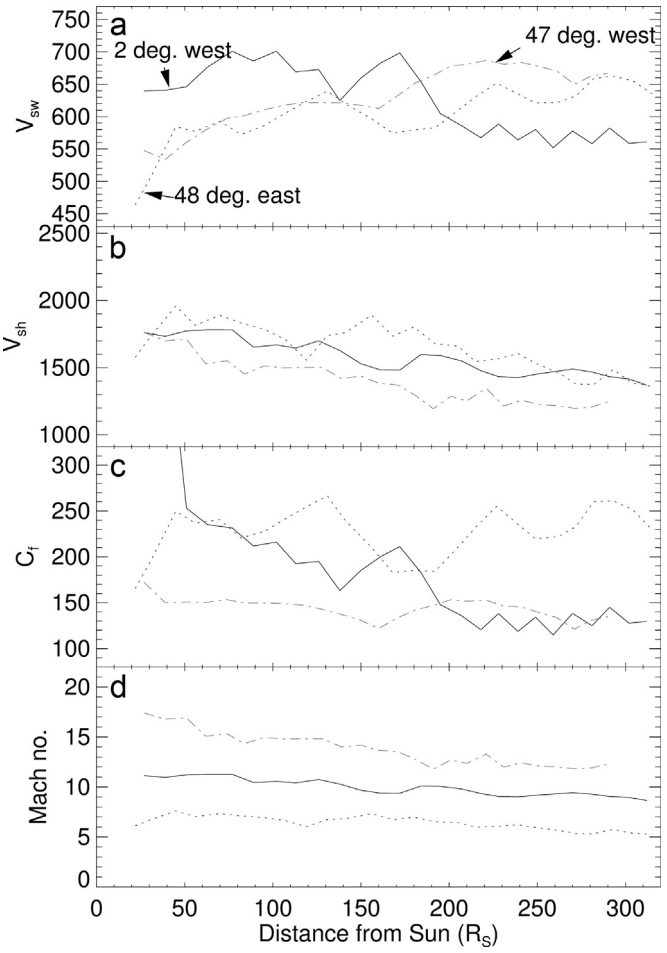

Fig. 7. (a) Solar wind speed upstream of the shock, (b) shock speed, (c) fast-mode magnetosonic wave speed in the solar wind frame, and (d) fast-mode Mach number as a function of radial distance from the Sun for three longitudes: 2°W (solid), 48°E (dotted), and 47°W (dashed-dot) of the CME initiation site.

4.4. Shock strength

For such a fast CME, one might expect a strong shock wave driven by the CME. In this subsection, we study temporal and spatial variations of the CME-driven shock. It is often assumed that the CME-driven shock front (at its "nose") is the fastest and strongest in shock strength. For the July 23 event, the CME was initiated in the active region, as it is also true for most other CME events in regions of high solar wind speed (see Fig. 4(a)). One would expect the shock to be faster along the radial direction at the initiation site because it is where the maximum power is presumably released. Here we test this hypothesis using the simulation result. Fig. 7 shows the solar wind speed upstream of the shock, the fast-mode shock wave speed relative to the solar wind, the wave speed for the fast-mode magnetosonic wave, and the Mach number for the fast-mode shock as a function of radial distance from the Sun for three locations: 2°W (black) (black),

48°E (purple), and 47°W (red) of the CME initiation site. Note that we use 2°W instead of 0° for the shock nose longitude because it is where the grid point is located. The calculation starts from 18 R_S because no plasma temperature information is available from the HAFv.2 code. The fast-mode magnetosonic wave speed (C_f) is defined, following Jackson (1975), as $C_f=(1/2)\ [C_s^2+V_A^2+\{(C_s^2+V_A^2)^2-4C_s^2V_A^2\cos^2\theta_{Bn}\}^{1/2}]$, where $C_s=(\gamma p/\rho)^{1/2}$ is the sound speed, $V_A=|\boldsymbol{B}|/(4\pi\rho)^{1/2}$ is the Alfvén speed, and θ_{Bn} is the angle between the upstream magnetic field ($\boldsymbol{B}$) and the shock normal. The fast-mode shock Mach number is defined as $M_f=V^*/C_f$, where V^* is the plasma speed in the solar wind frame ($V-V_s$). The shock speed is calculated as the time rate of the change of the shock location based on the wave transit method (Wu et al., 1996).

Fig. 7(a) shows the solar wind speed upstream of the shock. Indeed, it is faster at the CME initiation site than the other two regions away from this site. This can be seen in Fig. 4(a), until $r\sim 190R_S$. On the other hand, the fast-mode shock speed in the solar wind frame is about the same, but slightly faster in the east and slower in the west longitude (see Fig. 7(b)). Fig. 7(c) shows the fast-mode magnetosonic wave speed at the shock location. In general, the fast-mode wave is faster in the east than in the west longitude (200–250 km/s vs. ~150 km/s). Along the CME "nose," it is much faster initially but the speed drops below 150 km/s at ~190 R_S. Fig. 7(d) shows that the fast-mode shock Mach number at the three longitudes as a function of the radial distance from the Sun. The Mach number slowly decreases between 18R_S and ~1 AU. Interestingly, the fast-mode shock Mach number is the largest, ranging from 18 to 13, 45° west of the CME initiation location. The fast-mode shock Mach number is the smallest, ranging from ~8 to 5, 50° east of the CME initiation location. Along the CME nose the fast-mode shock number falls in between, ranging from ~11 to 9.

5. Discussion

5.1. Comparison with the Halloween events

Yashiro et al. (2004) showed statistically the average CME speed to be ~300 km/s in solar minimum and ~500 km/s in solar maximum. They also showed that less than 5% of the CME events observed by SOHO/LASCO were faster than 1000 km/s. The reported CME event on July 23, 2012, was obviously much faster than normal. Based on our simulation, the initial speed (at 2.5R_S) that is required to initiate the CME could exceed 3000 km/s. The two notable large CME events that occurred in the last decade, i.e. the events that occurred during the Halloween 2003 epoch, are only comparable in terms of their propagation speed. Table 1 shows the comparison of the three events. All three events occurred in the southern hemisphere ~15–16° from the solar equator. The two CME events during the Halloween epoch were halo-CMEs from the Earth's point of view, whereas the July 23, 2012 event was also a halo-CME event but from the STEREO-A point of view. The two Halloween events were associated with an X17.2 and an X10 flare, respectively. Because the present event occurred on the back-side, no flare measurement was available. The initial speed of the CME for the two Halloween events was 2000 km (Dryer et al., 2004). Based on our simulation results, the event under studied had an initial speed of ~3100 km/s, i.e., it was ~50% faster than the two Halloween events and is probably the fastest CME on record.

Table 1
Velocity pulse required to initiate shock/CME for Halloween 2003 and July 23 2012.

Event number	Type II start (date/time)	Arrival date/time (hh:mm)	Source[c]	Flare classification	Shock speed (km/s)
1[a]	2003-10-28/11:02	2003-10-29/05:58	S16E06	X17.2	2000
2[a]	2003-10-29/20:42	2003-10-30/16:19	S15E02	X10	2000
3	2012-07-23/02:50	2012-07-23/21:10[b]	S16W133		3100

[a] From Dryer et al. (2004).
[b] Arrival time at STEREO-A.
[c] The solar equatorial coordinate system is used for the source location.

The July 23, 2012, CME event was associated with the largest observed magnetic cloud in terms of its magnetic field strength. The magnetic field $|\boldsymbol{B}|$ recording at 1 AU (STEREO-A) is the largest (~110 nT) and is about 2 times of that for the Halloween event (e.g., Skoug et al., 2004). An interesting question is what would be the size of the storm if the 23 July 2012 CME/shock hit the Earth head on? Here we use a simple linear relationship formulated by linear least-squares fitting of the storm intensity (*Dst*) with magnetic cloud field data (Wu and Lepping, 2005): $Dst=0.83+7.85B_z(\text{min})$. For this event, the minimum southward IMF, B_z, was ~−47 nT at ~04 UT on July 24. This gives $Dst\sim-370$ nT. This formula would have probably underestimated the *Dst* index for the Halloween event ($Dst=-401$ nT) because the same formula would only have given $Dst\sim-376$ nT if B_z (min)~−35 nT were used. If the plasma flow speed within the magnetic cloud is considered the formula becomes: $Dst=-16.48-12.89\ (vB_s)_{\min}$, where vB_s is in mV/m. Here $(vB_s)_{\min}\sim(1500\text{ km/s})\times(47\text{ nT})=70$ mV/m, which gives $Dst\sim-885$ nT. This value is close to the estimate of −1000 nT made by Russell et al. (2013), who applied the formula by Burton et al. (1975) to this CME event if it would have hit the Earth. However, this value is likely overestimated because the same formula yields $Dst\sim-16.48-12.89\times(1400\text{ km/s}\times 35\text{ nT})\times 10^{-3}\sim-648$ nT for the Halloween event. By scaling the *Dst* linearly, using the value of the Halloween event, we found a *Dst* index of ~−545 nT, which is probably more reasonable and is closer to the estimate of −480 nT made by Baker et al. (2013). Note that both formulas predict a larger *Dst* value for the July 23, 2012 CME event than for the Halloween CME event if the Earth were located at STEREO's position. While it is not as large as the 1859 superstorm event, which probably produced *Dst*~−1760 nT (Tsurutani et al., 2003), it is comparable to the March 13, 1989 storm event ($Dst=-589$ nT), the largest storm of the 20th and, thus far, the 21th century.

5.2. Controlling factors of shock arrival time

The initial speed of the CME is probably one of the most important factors that determine the arrival time of the CME/shock at the Earth (and other places). The measurement of CME features in coronagraph images as employed in this study is limited to a projection of the "feature" onto the plane of the sky. In order to ascertain an accurate velocity, assumptions must be made about the actual direction of motion in three dimensions, and then a correction is applied to the measured values based on the inferred geometry. The lack of knowledge of this direction of motion is the largest contribution to uncertainty in the measured velocity. With a proper angle correction, the coronagraph images can provide reasonable estimates of the initial speed of CMEs, especially for large CME events; however, for small events, the technique may not work at all due to the sensitivity of the instrument. It has been shown that the measurement errors from the coronagraph technique increase with increasing distance from the Sun (Wen et al., 2007). This is the reason the present study adopted a model that uses $r=2.5R_s$ for the inner boundary of simulation domain. Note that current coronagraph cannot measure CMEs that are initiated within $2R_s$, where the CME-driven

shock may have been formed (e.g., Wu et al., 2012). It is also necessary to clarify that the coronagraph technique provides the CME speed not in the initial frame but in the solar wind frame. Within a few solar radii from the Sun, the plasma flow speed is expected to be small and the uncertainty is probably negligible for fast CMEs. Even for events with minimum uncertainties in the CME speed estimate, there is another uncertainty as demonstrated in this study. The uncertainty comes from the edge pixel selected. Different pixels result in different speeds. This is why different initial CME speeds were tested in our simulation until the shock arrival time matches the observations. It is also important to note that a good match in the shock arrival time does not mean a good match in the CME/shock distance and speed profile. This can only be confirmed with observations. The simulation result simply suggests a possible solution based on the simulation model and input parameters.

Our simulation also suggests that the ratio of specific heats affects the arrival time of the shock. A value of $\gamma=5/3$, which indicates adiabatic compression of monatomic gases, is widely used in global MHD simulations. Experimental measurements of γ have been conducted in many investigations (e.g., Fairfield, 1971; Chao and Wiskerchen, 1974), using the semi-invariant property of the standoff distance of the Earth's shock from the magnetopause at the stagnation point (Spreiter et al., 1966): $\Delta=1.1D\,(\rho/\rho')$, where D is the distance at the nose of the magnetopause from the center of the Earth and ρ/ρ' is the ratio of the mass density across the bow shock. These studies estimated the value of γ for the magnetosheath plasma ranging from ~1.5 to 2. While there is a clear difference between the Earth's bow shock and the CME-driven shock, there is no obvious reason to consider the two shocks to be associated with different thermodynamic processes. In other words, we cannot justify the γ value, but the use of $\gamma=5/3$ in our simulation should be adequate and provides the best estimate of the shock arrival time.

Our result clearly shows that the larger the γ value, the faster the shock speed. Differences in the arrival time from 1.25 to 1.67 are ~1.2 h. So the difference in the shock arrival time for typical γ values is not significant, as compared to the initial CME speed. Nonetheless, it is important to understand the effect of γ on the MHD CME/shock simulation. Recently, Wu et al. (2011) conducted a global simulation study of the CME event that occurred on August 3, 2010, using the same MHD model. They found that $\gamma=5/3$ provides a more accurate shock arrival time than $\gamma=1.45$. In this study, three γ values are investigated: 1.25, 1.45, and 1.67. In a good agreement with Wu et al. (2011), our simulation also shows better agreement between the simulated and measured shock arrival time when $\gamma=5/3$ is used. The effect of γ on the shock speed can be understood in thermodynamics physics. In a thermodynamic system, gas motion occurs due to unbalanced pressure. After being ejected from the Sun, the CME propagates outward and expands into a larger space due to a large pressure built behind the CME before the ejection. In our simulation model, we assume the solar wind/CME motion is an adiabatic process (i.e., $P\sim\rho\gamma$ with $\gamma=5/3$). Therefore, for the same solar mass density ejected from the Sun, a larger value of γ will result in a larger pressure in the CME, hence a faster CME/shock.

Note that we have not considered possible effects of the background solar wind speed. When a fast CME/shock propagates in a slow solar wind, the fluid drag can cause the CME/shock to slow down, thus delaying the shock arrival time. However, previous studies have suggested that the background solar wind shows little effect on the shock arrival time at Earth for solar disturbances (e.g., CME) with sufficiently large momentum inputs, e.g., $V(\text{peak})>1000$ km/s (e.g., Wu et al., 2005). As the CME event on 23 July 2012 is much faster ($V(\text{peak})>3000$ km/s), background solar wind effects may not be important and can be ignored. Recently, Liu et al. (2014) pointed out that the July 23 CME event was subject to a small deceleration. They suggested that a smaller solar wind drag for the event due to the removal of solar wind plasma by a preceding CME event on July 19 to be the cause.

5.3. Radial and longitudinal shock strength

The compression ratio (r) of the shock is also commonly used as the shock strength. In this study, we use the Mach number to categorize the shock strength along its periphery to demonstrate its importance as discussed in Section 4.4. The Mach number can be computed with parameters upstream of the shock. On the other hand, it requires parameters from both shock upstream and downstream to calculate the compression ratio. In a stationary planar shock, the two shock strength parameters are related through a simple function of γ. For large Mach numbers, the compression ratio can be simplified as $r=(1+\gamma)/(1-\gamma)$. Therefore, a smaller γ results in a larger compression ratio. Since the compression ratio is defined as the ratio of downstream to upstream gas density, the amplitude of the shock is directly controlled by γ. For a larger γ the solar wind density downstream of the shock (i.e., peak density) is smaller because of a smaller compression ratio. From the conservation of mass, the ratio of the downstream to upstream flow speed in the shock normal direction is reciprocally proportional to the compression ratio. Although this dependence is also shown in Fig. 6(b), the difference is not as pronounced as the solar wind density (not shown). This is because the compression ratio is computed based on the flow speed in the shock frame. When the shock speed is subtracted from the flow speed, the difference becomes clear (not shown). The behavior of the magnetic field at the shock is similar to that of the solar wind density because of the requirement of the frozen-in condition.

We also explore longitudinal variations of the shock strength. For this particular event, the shock strength is generally very large, with a Mach number greater than 5 for the three longitudes (2°W, 47°W, and 48°E of the CME initiation site). These values are indeed much greater than the typical Mach number (75% less than 2 and rarely greater than 4) for fast-mode shocks observed between 0.3 and 1 AU (Volkmer and Neubauer, 1985) and can easily put the shocked-solar wind in hypersonic flow category.

A surprisingly finding of the present simulation is that the shock Mach number is not the largest at the nose of the CME. Instead, it is larger in the west than in the east of the CME initiation longitude. Further analysis of the simulation result indicates that the true shock speed (in the solar wind frame) can be different, although the shock propagation speed is faster at the CME initiation longitudes. The Mach number, which is the ratio of the shock speed to the local wave speed, is not the largest at the CME initiation longitude, due to a larger local wave speed. CMEs are initiated at solar active regions where solar wind is faster (Zirker, 1997) and magnetic field is stronger. Closer to the Sun, the stronger magnetic field dominates the plasma dynamics. The fast-mode magnetosonic wave can be approximated by the Alfvén wave, which is proportional to the magnetic field strength. This is also demonstrated in Fig. 7(c). As a consequence, the shock strength is weaker. Because CME-driven shocks are considered the source of “gradual” solar energetic particle events (e.g., Reames, 1999; and references therein) it has recently been shown that the intensity of solar energetic particles (^{4}He and O) of greater than ~10 MeV is well correlated with the fast-mode shock Mach number (Liou et al., 2013). The present result suggests that the background solar wind plasma and magnetic field play an important role in the intensity of solar energetic particle (SEP) events through changing the shock strength. This latter topic is worth investigating but beyond the scope of the present work.

6. Conclusions

On July 23, 2012, a solar eruption from the active region AR 1520 produced a large CME event. Since this event was not directed toward Earth it had no space weather effects at all. In other words, it would have had space weather implications if it had impacted Earth. The CME was initiated backside and heading approximately toward the STEREO-A spacecraft. Both coronagraph and in situ measurements have recorded probably the largest CME event so far in solar cycle 24. We studied this CME event using a combined kinematic and MHD code, H3DMHD, to simulate the CME event. Our simulation study justifies the H3DMHD model's ability to handle extremely fast CME events. Thus, it was shown that there is generally good agreement between the observed and simulated total magnetic field strength and the plasma flow speed. Based on our simulation, the initial shock speed driven by the CME could have exceeded 3100 km/s and the shock transit speed at ~1 AU could have reached ~2000 km/s. An inaccurate estimate of the CME speed reduces the accuracy of the model prediction. It is also found that a smaller value of the adiabatic index tends to delay the arrival of the shock; however, the shock arrival time does not vary significantly over the typical values of the adiabatic index. Finally, we demonstrate the importance of the solar wind parameters in the shock strength along its periphery. We bring this point to the attention of the SEP community.

Acknowledgments

We are grateful to the Reviewers for their constructive comments on the paper. We acknowledge the use of solar EUV disk and coronagraph images from the STEREO/SECCHI instrument (R. A. Howard, PI), solar wind plasma data from STEREO/PLASTIC Investigation (A.B. Galvin, PI), and magnetic field data from STEREO/IMPACT (J. Luhmann, PI). The SECCHI data used here are produced by an international consortium of the Naval Research Laboratory, Lockheed Martin Solar and Astrophysics Laboratory, and NASA Goddard Space Flight Center (USA), Rutherford Appleton Laboratory and University of Birmingham (UK), Max-Planck-Institut für Sonnensystemforschung (Germany), Centre Spatiale de Liege (Belgium), Institut d′Optique Théorique et Appliqueé, and Institut d′Astrophysique Spatiale (France). The work at JHUAPL was supported partially by NSF Grant AGS-0964396. KL acknowledges support from APL's Janney grant for preparation of the manuscript. The work at NRL was supported by ONR 6.1 program. The work of S.-T. Wu is supported by NSF Grant AGS1153323 to UAH.

References

Acuna, M.H., Curtis, A.D., Scheifele, J.L., Russell, C.T., Schroeder, P., Szabo, A., Luhmann, J.G., 2008. The STEREO/IMPACT magnetic field experiment. Space Sci. Rev. 136, 203–226. http://dx.doi.org/10.1007/s11214-007-9259-2.

Akasofu, S.-I., 2011. A historical review of the geomagnetic storm-producing plasma flows from the Sun. Space Sci. Rev. 164, 85–132.

Arge, C.N., Pizzo, V.J., 2000. Improvement in the prediction of solar wind conditions using near-real time solar magnetic field updates. J. Geophys. Res. 105, 10,465–10,479. http://dx.doi.org/10.1029/1999JA000262.

Badruddin, F.M., 2013. Relative geo-effectiveness of coronal mass ejections with distinct features in interplanetary space. Planet. Space Sci. 82–83, 43–61. http://dx.doi.org/10.1016/j.pss.2013.03.011.

Baker, D.N., Li, X., Pulkkinen, A., Ngwira, C.M., Mays, M.L., Galvin, A.B., Simunac, K.D. C., 2013. Major solar eruptive event in July 2012: defining extreme space weather scenarios. Space Weather 11 (10), 585–591 (doi:0.1002/swe.20097).

Brueckner, G.E., et al., 1995. The Large Angle Spectroscopic Coronagraph (LASCO). Sol. Phys. 162, 357–402. http://dx.doi.org/10.1007/BF00733434.

Burlaga, L., Sittler, E., Mariani, F., Schwenn, R., 1981. Magnetic loop behind an interplanetary shock: Voyager, Helios, and IMP 8 observations. J. Geophys. Res. 86 (A8), 6673–6684. http://dx.doi.org/10.1029/JA086iA08p06673.

Burton, R.K., McPherron, R.L., Russell, C.T., 1975. An empirical relationship between interplanetary conditions and Dst. J. Geophys. Res. 80 (31), 4204–4214. http://dx.doi.org/10.1029/JA080i031p04204.

Carrington, R.C., 1859. Description of a singular appearance seen in the Sun on September. Mon. Notices R. Astron. Soc.XX, 13.

Chao, J.K., Wiskerchen, M.J., 1974. The ratio of specific heats for postshock plasmas of a detached bow shock: an MHD model. J. Geophys. Res. 79 (31), 4769–4774. http://dx.doi.org/10.1029/JA079i031p04769.

Cliver, E.W., Svalgaard, L., 2004. The 1859 Solar–Terrestrial disturbance and the current limits of extreme space weather activity. Solar Physics 224 (1-2), 407–422.

Detman, T.R., Dryer, M., Yeh, T., Han, S.M., Wu, S.T., 1991. A time-dependent, three-dimensional MHD numerical study of interplanetary magnetic draping around plasmoids in the solar wind. J. Geophys. Res. 96, 9531–9540. http://dx.doi.org/10.1029/91JA00443.

Dryer, M., 1981. Solar-generated disturbances and their propagation through the interplanetary medium. In: Rosenbauer, H. (Ed.), Proceedings of the Fourth Solar Wind Symposium. Max-Planck Inst. fur Aeronomie, Rpt. MPAE-W-100-81-31, October, pp. 199–210.

Dryer, M., Smith, Z., Fry, C.D., Sun, W., Deehr, C.S., Akasofu, S.-I., 2004. Real-time shock arrival predictions during the "Halloween 2003 epoch". Space Weather 2, S09001. http://dx.doi.org/10.1029/2004SW000087.

Dryer, M., Liou, K., Wu, C.-C., Wu, S.-T., Rich, N., Plunkett, S., Simpson, L., Fry, C.D., Schenk, K., 2012. Extreme fast coronal mass ejection on 23 July 2012. Presented at 2012 Fall Meeting. AGU, San Francisco, California, 3–7 December, Abstract SH44B-04.

Fairfield, D.H., 1971. Average and unusual locations of the earth's magnetopause and bow shock. J. Geophys. Res. 76, 6700. http://dx.doi.org/10.1029/JA076i028p06700.

Fry, C.D., Sun, W., Deehr, C.S., Dryer, M., Smith, Z., Akasofu, S.-I., Tokumaru, M., Kojima, M., 2001. Improvements to the HAF solar wind model for space weather predictions. J. Geophys. Res. 106 (A10), 20985–21001. http://dx.doi.org/10.1029/2000JA000220.

Galvin, A.B., 2008. The Plasma and Suprathermal Ion Composition (PLASTIC) investigation on the STEREO observatories. Space Sci. Rev. 136 (1–4), 437–486. http://dx.doi.org/10.1007/s11214-007-9296-x.

Gopalswamy, N., Lara, A., Manoharan, P.K., Howard, R.A., 2005. An empirical model to predict the 1-AU arrival of interplanetary shocksAdv. Space Res. 36 (12), 2289–2294.

Gosling, J.T., McComas, D.J., Phillips, J.L., Bame, S.J., 1991. Geomagnetic activity associated with earth passage of interplanetary shock disturbances and coronal mass ejections. J. Geophys. Res. 96 (A5), 7831–7839. http://dx.doi.org/10.1029/91JA00316.

Hakamada, K., Akasofu, S.-I., 1982. Simulation of three-dimensional solar wind disturbances and resulting geomagnetic storms. Space Sci. Rev. 31 (1), 3–70. http://dx.doi.org/10.1007/BF00349000.

Han, S.M., 1977. A Numerical Study of Two Dimensional Time-dependent Magnetohydrodynamic Flows (Ph.D. thesis). University of Alabama, Huntsville.

Han, S.M., Wu, S.T., Dryer, M., 1988. A three-dimensional, time-dependent numerical modeling of super-sonic, super-Alfvénic MHD flow. Comput. Fluids 16, 81–103. http://dx.doi.org/10.1016/0045-7930(88)90040-0.

Jackson, J.D., 1975. Classical Electrodynamics. John Wiley & Son, New York.

Lax, P.D., Wendroff, B., 1960. Systems of conservation laws. Commun. Pure Appl. Math. 13, 217–237. http://dx.doi.org/10.1002/cpa.3160130205.

Liou, K., Wu, C.-C., Dryer, M., Wu, S.-T., Berdichevsky, D.B., Plunkett, S., Mewaldt, R. A., Mason, G.M., 2013. Magnetohydrodynamic fast shocks and their relation to solar energetic particle event intensities. Terr. Atmos. Ocean. Sci. 24, 165–173. http://dx.doi.org/10.3319/TAO.2012.05.08.01(SEC).

Lugaz, N., Roussev, I.I., 2011. Numerical modeling of interplanetary coronal mass ejections and comparison with heliospheric images. J. Atmos. Sol.–Terr. Phys. 73 (10), 1187–1200. http://dx.doi.org/10.1016/j.jastp.2010.08.016.

Manchester, W.B., Gombosi, T.I., Roussev, I., Ridley, A., Zeeuw, D.D., Sokolov, I.V., Powell, K.G., Toth, G., 2004. Modeling a space weather event from the Sun to the Earth: CME generation and interplanetary propagation. J. Geophys. Phys. 109, A02107. http://dx.doi.org/10.1029/2003JA010150.

MacQueen, R.M., Csoeke-Poeckh, A., Hildner, E., House, L., Reynolds, R., Stanger, A., Tepoel, H., Wagner, W., 1980. The high altitude observatory coronagraph/polarimeter on the solar maximum mission. Sol. Phys. 65, 91–107.

Odstrcil, D., Pizzo, V.J., Arge, C.N., 2005. Propagation of the 12 May 1997 interplanetary coronal mass ejection in evolving solar wind structures. J. Geophys. Phys. 110, A02106. http://dx.doi.org/10.1029/2004JA010745.

Reames, D.V., 1999. Particle acceleration at the Sun and in the heliosphere. Space Sci. Rev. 90, 413–491. http://dx.doi.org/10.1023/A:1005105831781.

Russell, C.T., Mewaldt, R.A., Luhmann, J.G., Mason, G.M., von Rosenvinge, T.T., Cohen, C.M.S., Leske, R.A., Gomez-Herrero, R., Klassen, A., Galvin, A.B., Simunac, K.D.C., 2013. The very unusual interplanetary coronal mass ejection of 2012 July 23: a blast wave mediated by solar energetic particles. Astrophys. J. 770 (38), 1–5. http://dx.doi.org/10.1088/0004-637X/770/1/38.

Sheeley, N.R.,,J.R., et al., 2008. Thliospheric images of the solar wind at Earth. Astrophys. J. 675, 853–862.

Shen, F., Feng, X.S., Wu, S.T., Xiang, C.Q., Song, W.B., 2011. Three-dimensional MHD simulation of the evolution of the April 2000 CME event and its induced shocks using a magnetized plasma blob model. J. Geophys. Res. 116, A04102. http://dx.doi.org/10.1029/2010JA0158.

Liu, Y.D., et al., 2014. Observations of an extreme storm in interplanetary space caused by successiove coronal mass ejections. Nat. Commun. 5, 3481. http://dx.doi.org/10.1038/ncomms4481.

Skoug, R.M., Gosling, J.T., Steinberg, J.T., McComas, D.J., Smith, C.W., Ness, N.F., Hu, Q., Burlaga, L.F., 2004. Extremely high speed solar wind: 29–30 October 2003. J. Geophys. Res. 109, A09102. http://dx.doi.org/10.1029/2004JA010494.

Spreiter, J.R., Summers, A.L., Alksne, A.Y., 1966. Hydromagnetic flow around the magnetosphere. Planet. Space Sci. 14, 223.

Tsurutani, B.T., Gonzalez, W.D., Lakhina, G.S., Alex, S., 2003. The extreme magnetic storm of 1–2 September 1859. J. Geophys. Res. 108, 1268. http://dx.doi.org/10.1029/2002JA009504 A7.

Tousey, R., 1973. The solar corona. In: Rycroft, M.J., Runcorn, S.K. (Eds.), Space Research XIII, Proceedings of Open Meetings of Working Groups on Physical Sciences of the 15th Plenary Meeting of COSPAR, Madrid, Spain, 10–24 May. Akademie-Verlag, Berlin, pp. 713–730.

Volkmer, P.M., Neubauer, F.M., 1985. Statistical properties of fast magnetoacoustic shock waves in the solar wind between 0.3 AU and 1 AU-Helios-1, 2 observations. Ann. Geophys. 3, 1–12.

Wen, Y., Maia, D.J.F., Wang, J., 2007. The CME acceleration problem: error estimates in LASCO coronal mass ejection measurements. Astrophys. J. 657, 1117–1126. http://dx.doi.org/10.1086/507405.

Wu, C.-C., Lepping, R.P., 2011. Statistical comparison of magnetic clouds with interplanetary coronal mass ejections for solar cycle 23. Sol. Phys. 269, 141–153. http://dx.doi.org/10.1007/s11207-010-9684-3.

Wu, C.-C., Dryer, M., Wu, S.T., 1996. Three-dimensional MHD simulation of interplanetary magnetic field changes at 1 AU as a consequence of simulated solar flares. Ann. Geophys. 14 (4), 383–399 (doi:20.1007/s00585-996-0383-1).

Wu, Chin-Chun, Fry, C.D., Wu, S.T., Dryer, M., Liou, K., 2007. Three-dimensional global simulation of ICME propagation from the Sun to the heliosphere: 12 May 1997 solar event. J. Geophys. Res. 112, A09104. http://dx.doi.org/10.1029/2006JA012211.

Wu, C.C., Wu, S.-T., Liou, K., Plunkett, S., 2012. Evolution of a magnetohydrodynamic coronal shock, in space weather: the pace radiation environment: 11th annual international astrophysics conference. AIP Conf. Proc. 1500 (2012), 50. http://dx.doi.org/10.1063/1.4768744.

Wu, C.-C., Lepping, R.P., 2002. Effects of magnetic clouds on the occurrence of geomagnetic storms: the first 4 years of Wind. J. Geophys. Res. 107 (A10), 1314. http://dx.doi.org/10.1029/2001JA000161.

Wu, C.-C., Lepping, R.P., 2005. Relationships for predicting magnetic cloud-related geomagnetic storm intensity. J. Atmos. Sol.–Terr. Phys. 67, 283–291.

Wu, C.-C., Fry, C.D., Berdichevsky, D., Dryer, M., Smith, Z., Detman, T., 2005. Predicting the arrival time of shock passages at Earth. Sol. Phys. 227, 371–386. http://dx.doi.org/10.1007/s11207-005-1213-4.

Wu, C.-C., Dryer, M., Wu, S.T., Wood, B.E., Fry, C.D., Liou, K., Plunkett, K., S., 2011. Global three-dimensional simulation of the interplanetary evolution of the observed geoeffective coronal mass ejection during the epoch 1–4 August 2010. J. Geophys. Res. 116, A12103. http://dx.doi.org/10.1029/2011JA016947.

Yashiro, S., Gopalswamy, N., Michalek, G., Cyr St., O.C., Plunkett, S.P., Rich, N.B., Howard, R.A., 2004. A catalog of white light coronal mass ejections observed by the SOHO spacecraft. J. Geophys. Res. 109, A07105. http://dx.doi.org/10.1029/2003JA010282.

Yermolaev, Y.I., Yermolaev, M.Y., 2006. Statistic study on the geomagnetic storm effectiveness of solar and interplanetary events. Adv. Space Res. 37 (6), 1175–1181.

Zastenker, G.N., Temnyi, V.V., Duston, C., Bosqued, J.M., 1978. The form and energy of the shock waves from the solar flares of August 2, 4, and 7, 1972. J. Geophys. Res. 83 (A3), 1035–1041. http://dx.doi.org/10.1029/JA083iA03p01035.

Zhang, J.-Ch., Liemohn, M.W., Kozyra, J.U., Lynch, B.J., Zurbuchen, T.H., 2004. A statistical study of the geoeffectiveness of magnetic clouds during high solar activity years. J. Geophys. Res. 109, A09101. http://dx.doi.org/10.1029/2004JA010410.

Zirker, J.B., 1997. Coronal holes and high-speed wind streams. Rev. Geophys. Space Phys. 15, 257–269. http://dx.doi.org/10.1029/RG015i003p00257.